Korean J. Chem. Eng., **28**(10), 2033-2040 (2011)
DOI: 10.1007/s11814-011-0072-y

Biosorption of copper(II) on prunus amygdalus shell: Characterization, biosorbent size analysis, kinetic, equilibrium and mechanistic studies

Mohsin Kazmi†, Nadeem Feroze, Shahid Naveed, and Syed Hassan Javed

Department of Chemical Engineering, University of Engineering &Technology, Lahore 54890, Pakistan
(*Received 24 February 2011 • accepted 21 March 2011*)

Abstract−Deletion of Cu(II) from synthetic solution was investigated using ground Prunus Amygdalus shell (GPAS). FTIR revealed the probable functional groups for the binding of Cu(II). XRD revealed amorphous nature of the GPAS. SEM analysis furnished microscopic details of GPAS. GPAS size analysis was done using seven ASTM screens and three mean diameters, namely mass mean, volume mean and volume surface mean diameters. Kinetic study consisted of pseudo-first and pseudo-second order kinetics. Langmuir and Freundlich isotherms were used to elucidate the isotherm study of uptake of Cu(II) onto GPAS. Trend of Scatchard was used to verify the applicability of the Freundlich model, while D-R model helped to determine the nature of biosorption. A detailed analysis for rate controlling step was made. Various mean diameters were used to estimate the diffusion coefficient for the biosorption of Cu(II) onto GPAS.

Key words: Prunus Amygdalus Shell, Biosorption, Characterization, Equilibrium, Kinetics, Mechanistic Studies, Size Analysis

INTRODUCTION

Heavy metals mobilized and released into the atmosphere by industrial activities like mining, electroplating, tanning, pulp and paper etc have a tendency to endure for an indefinite period, circulating and finally accumulating throughout the food chain, thus appearing as a lethal threat to all the livings and their surroundings [1]. Drinking water and wastewater contaminated with cadmium, copper, lead, nickel and zinc is a serious ongoing issue in this context [2].

Copper finds extensive applications in industries like air conditioning tubing and roofing, gear wheel, electrical winding, plumbing and selenium rectifier because of its tremendous physical properties of electrical and thermal conductivity, corrosion resistivity, ease of manufacturing and installation. Copper is an important element for all types of living in trace value. On the other hand, disproportionate copper can be harmful for the environment. Therefore, removal of copper from wastewater is indispensable not only to care for water assets but also to decelerate the rate of loss of copper reserves. Fertilizer industry, wood pulp production, printed circuit board production, paper board mills and metal cleaning and plating baths are some sources of copper effluents [3-5].

The best way to remediate heavy metal contaminated water is to treat it at source, i.e., before dispersion of wastewater to multifarious ecosystems [4]. To achieve this goal a list of conventional technologies like membrane separation, sedimentation, evaporation, precipitation/sedimentation, adsorption, etc., is available. All these technologies can sequester or concentrate heavy metals from the polluted water, but they face economical and practical limitations like repeated alteration of filter, production of large volume of sludge which again requires safest disposal [1,3-5].

Over the past few decades biosorption has been extensively investigated as a potential candidate for removal of toxic heavy metals, especially at low concentration, i.e., less than 100 ppm [6-8]. In biosorption passive removal of toxic heavy metals results due to bonding between binding sites of dead biomass and metallic species through various mechanisms [9]. Industrial sludge, agricultural waste and dead microorganisms (like fungi, algae and bacteria) are three basic types of biomasses opted for the metal sequestration [10-12]. Brewery biomass, green algae, brown algae, saw dust, Peanut hull, rice straw, and activated carbon derived from apricot stone, rice husk, almond, pistachio, hazelnut and walnut shells [3,13-18] are few examples of low cost biosorbents used for removal of various heavy metals.

In this work ground Prunus Amygdalus shell has been used to present a mechanistic and mass transfer study for the deduction of Cu(II) from aqueous solution. Although in all works related to heavy metals removal using dead biomasses, particle size of the biosorbent is mentioned but rarely detailed size analysis is presented. Therefore, the basic objectives of this study are to (i) characterize GPAS, (ii) present detailed size analysis of the GPAS, (iii) present kinetic and equilibrium studies to understand basic mechanism of copper removal by GPAS, and (iv) determine the rate controlling step.

MATERIALS AND METHODS

1. Materials

1-1. Chemicals & Methods

Analytical grade chemicals were used for the study. Synthetic solution of 1,000 ppm was prepared by dissolving copper nitrate ($Cu(NO_3)_2 \cdot 5H_2O$). This solution was further diluted to various known concentrations of copper ions for different experiments using micropipette. An orbital shaker with heating water bath was used for batch experiments at 120 rpm and temperature was adjusted at 30±2 °C. It has capacity to hold eight 250 mL Erlenmeyer flasks. In kinetic studies Cu(II) initial concentration was 100 ppm. Flasks were with-

†To whom correspondence should be addressed.
E-mail: engr.smalikazmi@gmail.com

drawn from orbital shaker after providing a shaking time of 1, 2, 3, 5, 6, 8, and 15 minutes. In equilibrium studies 2, 3, 5, 10, 15, 30, 45, 60, 85 and 100 ppms were taken as initial concentrations and pH was measured by a digital pH meter and was maintained around 5. In all experiments 100 mL of adsorbate was used and concentration of biosorbent was kept at 1 gL^{-1}. All experiments were performed in triplicate and average values with 4-5% deviation were used in all calculations. Simple filtration was performed to separate biosorbent from solution preceded by a short settling time (2-3 minutes). Unknown concentrations of copper were determined by atomic absorption spectrophotometer (Shimadzu 6800) using an air-acetylene flame.

2. Biomass Preparation and Characterization

Ground Prunus Amygdalus shell (GPAS) was obtained through crushing and grinding, in a double roll crusher and a spice grinder respectively, of the Prunus Amygdalus shells after they were washed with distilled water and dried in shade. A stack of seven ASTM screens was used to establish the size distribution of the product.

To characterize the functional groups present on GPAS, Fourier transform infrared spectroscopy analysis was performed by JASCO FT-IR 4000 using KBr with 2% finely ground sample. Infrared spectra were recorded in the region of 400 cm^{-1} to 4,000 cm^{-1}.

XRD measurements were performed on a Philips Model PANalytical X'Pert Pro system with copper anode X-Ray tube (PW3373/00 Cu LFF DK147356). The Kα radiation (λ=0.1540 nm) was selected with a diffracted beam monochromator at 45 kV and 40 mA. X-ray patterns were observed in a 2θ range between 5° and 120° at a step size of 0.025° with incident beam path 240 mm.

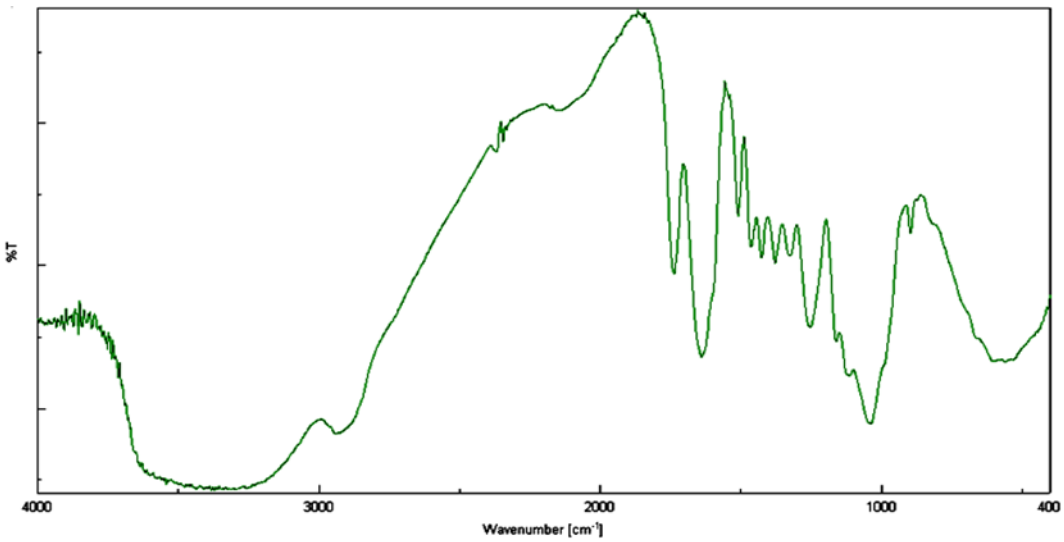

Fig. 1. FT-IR analysis of GPAS.

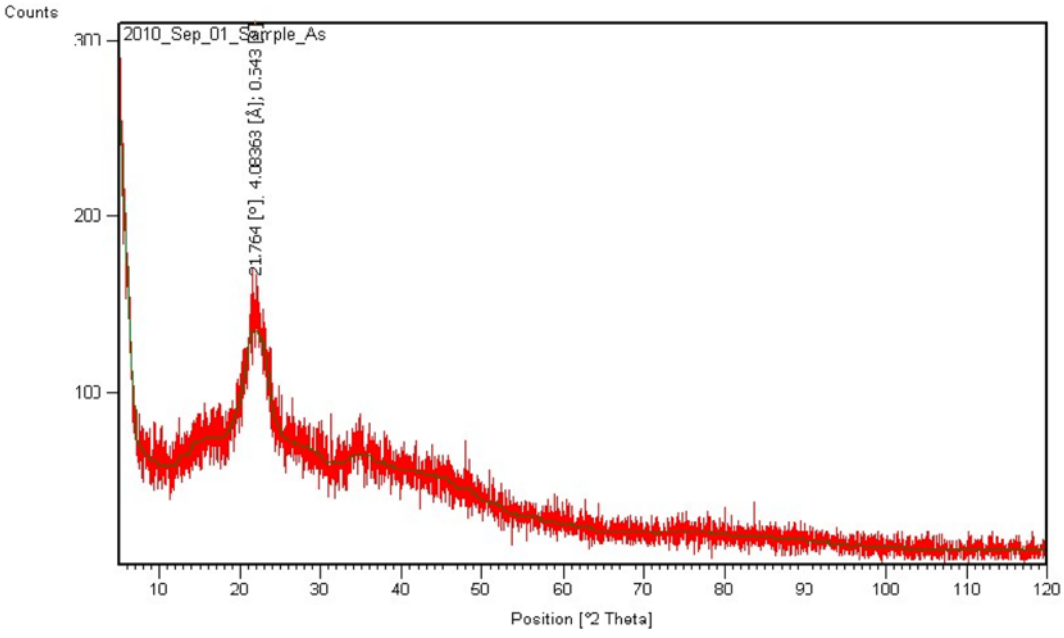

Fig. 2. XRD spectrum of GPAS.

To characterize the surface morphology, particle size and shape GPAS particles were coated with a thin layer of graphite and observed by an SEM (JEOL JSM-6490 LV).

RESULTS AND DISCUSSION

1. Characterization

1-1. FT-IR Analysis

FT-IR analysis was performed to characterize the functional groups which could be accountable for the metal uptake by GPAS, as shown in Fig. 1. Thus a complex nature of GPAS may be observed. A broad stretch at 2,937.06 cm^{-1} and peaks at 1,379.82 cm^{-1}, 1,421.28 cm^{-1} and 1,470.46 cm^{-1} showed bending and scissoring of the C-H bonds for saturated groups, respectively. Peaks at 1,509.99 cm^{-1} and 1,632 cm^{-1} correspond to C=C of aromatic compounds. Stretches at 1,040.41 cm^{-1}, 1,116.58 cm^{-1}, 1,166.72 cm^{-1} and 1,254.47 cm^{-1} showed the presence of carbonyl groups (C-O) for ethers and carboxylic acids. A strong stretch at 1,734.66 cm^{-1} confirmed the presence of carboxylic acid (C=O) group. A broad peak between 3,600-3,200 cm^{-1} showed the presence of hydrogen bonded alcoholic groups. These functional groups corresponded to the presence of compounds like cellulose and pectin [7,19].

1-2. XRD Analysis

The XRD pattern of GPAS is presented in Fig. 2. It indicates the typical amorphous behavior with a peak ~22°. Some polymers show amorphous region as a result of their inability to generate definite XRD lines. Fig. 2 does not exhibit any mineral phase, which may be due to either their very low concentration or masking of inorganic phase by the organic matter [20].

1-3. SEM Analysis

Fig. 3 shows the SEM image of GPAS used in the experiments. Fig. 3(a) and (b) show that there were two types of particles which participated in the biosorption of Cu(II) onto GPAS: irregular particles or their agglomerates, and fibrils of Prunus Amygdalus shell. It can be seen that the amount of fibrils is less than that of other irregular particles or their agglomerates. Therefore, consideration was given to agglomerates for size and shape analysis as shown in Fig. 3(c). It shows that GPAS biosorbent is composed of irregular shape particles in wide range. Majority of the particles were roughly 3 to 4 times larger when compared to the 10 μm micron-marker as shown in Fig. 3(c). This particle size distribution has been further elaborated through detailed size analysis.

2. Screening and Size Analysis

Particle size distribution influences the handling and metal uptake characteristics of the biosorbents. Normally, a material with smaller average particle size exhibits faster kinetics and higher uptakes [8]. Estimation of average particle size helps in understanding mass transfer mechanism through calculation of various parameters like diffusion coefficient [21]. Different average diameters can be calculated based on different aspects of particle geometry. A good estimation of average diameter is one which corresponds to size frequency curve [22]. To perform size analysis, ground material was sieved through seven ASTM screens. Table 1 shows the cumulative size analysis smaller than D_p (screen opening). First column of Table 1 shows the clear opening of the ASTM screen used in the analysis. Second column indicates the mass fraction retained on the corresponding screen. Values in third column are obtained by the arithmetic mean

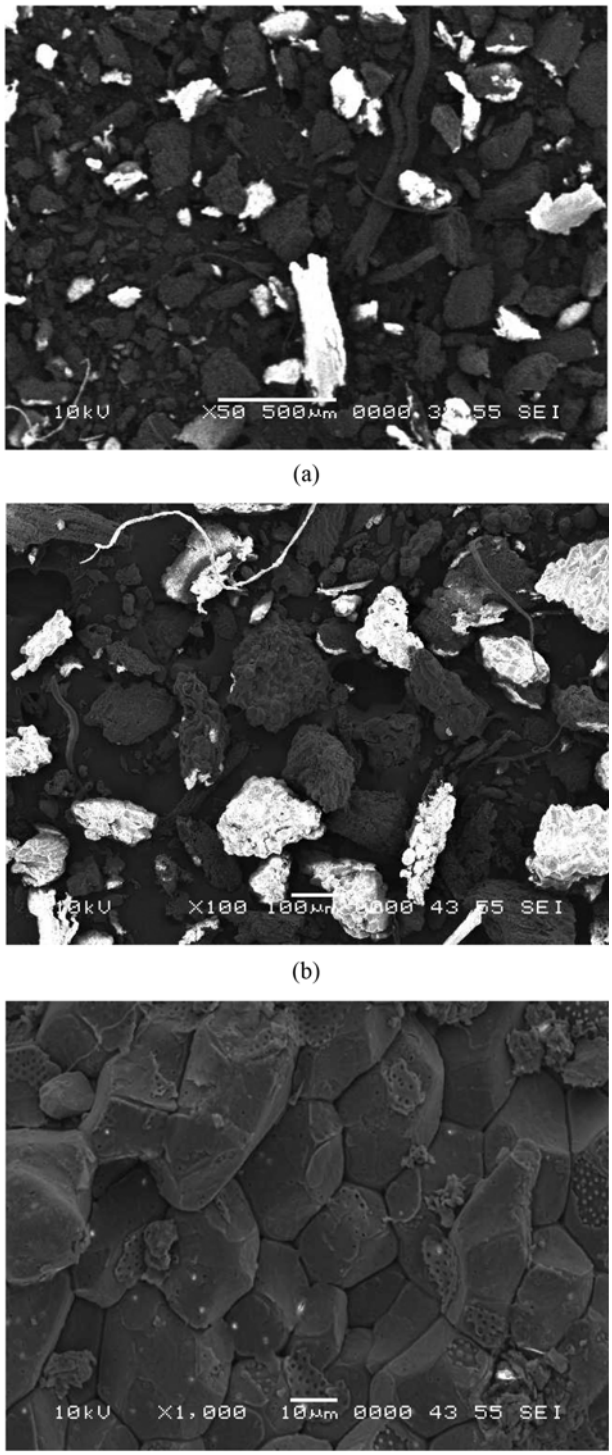

Fig. 3. SEM images of GPAS at 50×, 100× and 1,000× after Cu(II) adsorption.

of clear openings of the successive screens. Fourth column presents the cumulative mass fraction (C.M.F.) obtained by successive addition of the individual mass fractions, starting from bottom to top hence assigning the size that of larger clear opening. A size frequency curve is shown in Fig. 4. Median size determined from Fig. 4 is 0.041 mm. Different average diameters, namely volume sur-

Table 1. Size distribution and average diameters calculation of GPAS

Screen opening (mm)	Mass fraction (xi)	Average diameter ($\overline{D}_{pi}$, mm)	C.M.F. X
0.212	0.000	------	1.000
0.152	0.313	0.182	0.687
0.106	0.086	0.129	0.601
0.053	0.066	0.080	0.536
0.044	0.018	0.049	0.518
0.037	0.048	0.041	0.470
0.025	0.470	0.031	0.000
Average diameters			
$\overline{D}_s$	0.051 mm		
$\overline{D}_m$	0.091 mm		
$\overline{D}_v$	0.039 mm		

face mean diameter, mass mean diameter and volume mean diameter [22], were calculated as shown in Table 1.

$$\text{Volume surface mean diameter} = \overline{D}_s = \frac{1}{\sum_i^n (x_i/\overline{D}_{pi})} \quad (1)$$

$$\text{Mass mean diameter} = \overline{D}_m = \sum_i^n x_i \overline{D}_{pi} \quad (2)$$

$$\text{Volume mean diameter} = \overline{D}_v = \left[\frac{1}{\sum_i^n (x_i/\overline{D}_{pi}^3)}\right]^{1/3} \quad (3)$$

It is seen that volume mean diameter is close to the median value of the size obtained from the Fig. 4. Hence, it can be deduced that the volume mean diameter represents the system under consideration.

3. Adsorption Kinetic Study

Fig. 5 illustrates the effect of contact time on uptake of copper by GPAS. It can be seen that by increasing contact time the adsorption of copper is increased and reaches to equilibrium in less than 10 minutes. After 10 minutes an increase in contact time resulted in a slight lowering of uptake of copper ions. Three steps could be identified: (i) initial fast step where uptake was fast and contributed

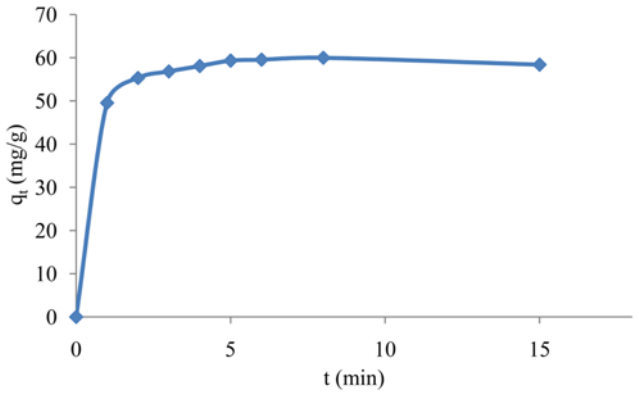

Fig. 5. Effect of contact time on uptake of Cu^{2+} (C=100 ppm) by GPAS.

significantly to equilibrium uptake, (ii) second sluggish step whose contribution to total uptake was comparatively small, and (iii) a slight declining step [23]. The trend in Fig. 5 can be interpreted as in the start large adsorption sites were available due to which rapid removal of copper ions took place through surface adsorption, followed by a slower step due to intra-particle diffusion through particle. Liquid film developed on the biosorbent offered resistance in the uptake of Cu(II) onto GPAS [16]. Slight lowering of copper adsorption suggested the establishment of equilibrium in less than ten minutes. A contact time of 8 minutes was concluded as equilibrium time for the biosorption of Cu(II) onto GPAS.

3-1. Adsorption Kinetic Modeling

Kinetics models are used to elaborate the adsorption mechanism and important adsorption parameters like order of kinetics, rate constant, initial adsorption rate, rate controlling step, diffusion coefficient etc [3,10]. Two simple kinetic models were used to determine the order of the rate of adsorption: pseudo-first order and pseudo-second order kinetics.

3-1-1. Pseudo First Order Kinetic

The pseudo-first order rate equation is represented by the following linearized expression [13]:

$$\log(q_e - q_t) = \log q_e - k_1 t \quad (4)$$

where q_e and q_t are the uptakes of solute ($mg \cdot g^{-1}$) at equilibrium and time t (min), respectively, while k_1 is kinetic rate constant of

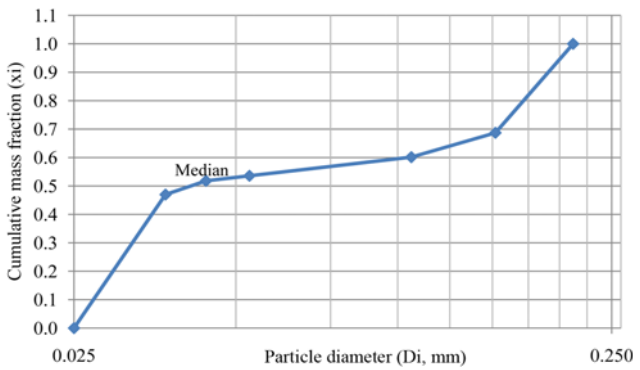

Fig. 4. Cumulative curve smaller than D_p. Median value is 0.041 mm.

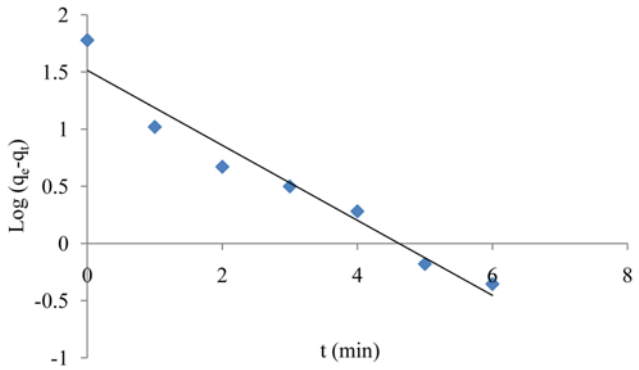

Fig. 6. Test of pseudo first order equation for the adsorption of Cu^{2+} ions onto GPAS from aqueous solution (100 ppm).

pseudo-first adsorption. This model is for adsorption in liquid/solid system based on biosorbent capability of metal removal and assumes that rate of metal removal is directly proportional to the change of equilibrium uptake and the amount of solid uptake with time [3]. Fig. 6 shows the linear fit of $\log(q_e - q_t)$ versus t. The R^2 value for this case is 0.9518, which means biosorption of Cu(II) onto GPAS does not follow the pseudo-first order kinetics. To find a reliable explanation of the kinetics, second-order kinetic was applied.

3-1-2. Pseudo-second Order Kinetic

The pseudo-second order rate equation is given by:

$$\frac{t}{q_t} = \frac{t}{q_e} + \frac{1}{k_2 q_e^2} \quad (5)$$

where k_2 is pseudo-second order rate constant ($g \cdot mg^{-1} \cdot min^{-1}$). The term $k_2 q_e^2$ represents the initial rate of adsorption. This model is based on the assumption that the rate of coverage of adsorption sites is directly related to the square of the uncovered adsorption sites [3]. A plot of t/q_t versus t yielded a linear line with correlation coefficient of 0.9993 as shown in Fig. 7. Parameters for pseudo-second order kinetics are given in Table 3.

It was observed that theoretically calculated q_e value based on pseudo-second order kinetic was very close to the experimental value with less than 2% deviation at the given conditions. We thus concluded that adsorption of Cu^{2+} ions on GPAS follows 2^{nd} order rate kinetics.

4. Adsorption Equilibrium Study

Adsorption equilibrium study was performed by varying Cu^{2+} concentration (1-100 ppm) for 8 minutes as shown in Fig. 8. It was noticed that performance of biosorbent is highly affected by the initial concentration. Increasing the initial concentration from 2 to 100 ppm, the removal efficiency was decreased from 98% to 60% and the adsorption capacity increased from 0.98 mg/g to 59.98 mg/g. The decrease in removal efficiency of Cu^{2+} can be interpreted as biosorbent had a limited number of adsorption sites, which would have become occupied after a certain concentration. The increase in uptake of Cu^{2+} with higher initial concentration could be due to the greater adsorption rate and coverage of all the sorption sites available for the biosorption [16].

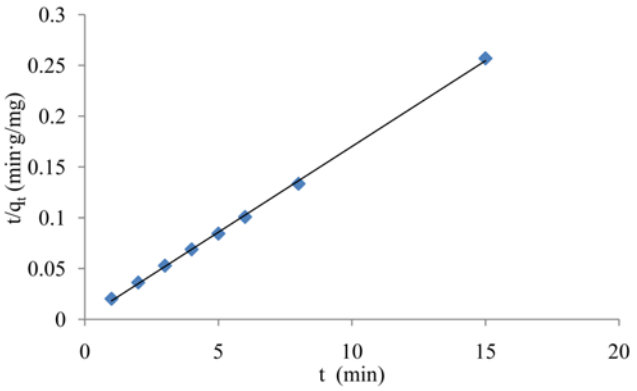

Fig. 7. Pseudo second order model for the adsorption of Cu^{2+} ions onto GPAS from aqueous solution (100 ppm).

Table 2. Parameters of pseudo 1st order kinetic

k_1	−0.3281
$\log(q_{e,\,Exp})$	1.78
$\log(q_{e,\,Cal})$	1.515
R^2	0.9518

Table 3. Parameters of pseudo 2nd order kinetic

$q_{e,\,Exp}$	59.9803
$q_{e,\,Cal}$	59.2461
h	749.4101
R^2	0.9993

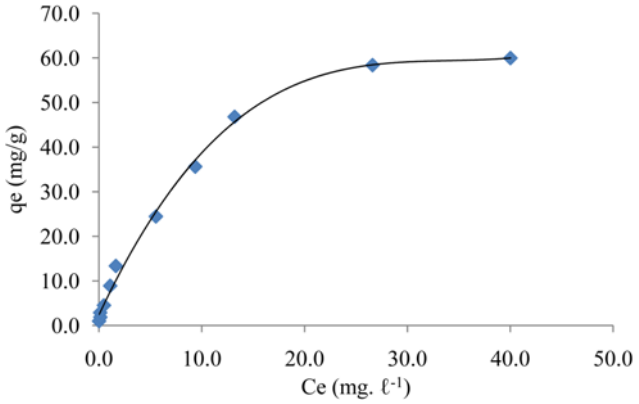

Fig. 8. Sorption isotherm of Cu^{2+} ion on GPAS as a function of initial Cu^{2+} concentration.

4-1. Adsorption Equilibrium Modeling

Adsorption models provide a simple means to enumerate the adsorption mechanism for the interaction of Cu^{2+} on the biosorbent surface. An adsorption isotherm model is characterized by different constants, which provides a quick explanation of surface properties and the affinity of the biosorbent for the metals (Cu^{2+}). Langmuir and Freundlich isothermal models [24] were employed to study the biosorption process.

Langmuir model is true for monolayer sorption of metal ions on to finite number of identical sorption sites and is given by the following equation:

$$\frac{q_{eq}}{q_{max}} = \frac{bC_{eq}}{1 + bC_{eq}} \quad (6)$$

Where b and q_{max} are Langmuir constants expressing the equilibrium constant for the adsorbate - adsorbent equilibrium and the monolayer capacity, respectively. These constants can be determined by the slope and intercept of the following linearized Langmuir isotherm:

$$\frac{C_e}{q_e} = \frac{1}{bq_{max}} + \frac{C_e}{q_{max}} \quad (7)$$

A linear plot between C_e/q_e versus C_e is shown in Fig. 9. Values of q_{max} and b were 70.16 mg/g and 0.1469. Langmuir model gave a good fitting to the data of copper ion sorption onto GPAS as shown by correlation coefficient (R^2=0.9772).

Unlike Langmuir, the Freundlich isotherm assumes presence of multiple adsorption sites on the biosorbent and is given by the following expression:

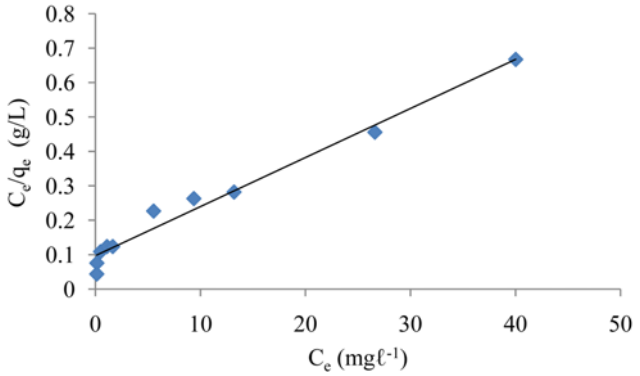

Fig. 9. Langmuir isotherm model for the Cu^{2+} sorption onto GPAS.

$$q_e = K_f C_e^{1/n} \quad (8)$$

Here K_f is Freundlich constant (mg·g^{-1}); n the affinity constant. Linearized form of Freundlich model is as below:

$$\log q_e = \log K_f + \frac{\log C_e}{n} \quad (9)$$

A plot of log q_e and logC_e is given in Fig. 10. It is clear that the Freundlich model gave better fit with higher correlation coefficient (R^2=0.9892). Values of n and K_f were 1.64 and 8.19 as calculated from the slope and intercept of the plot in Fig. 10. According to this model a value of n between 1 and 10 corresponds to favorable adsorption [25].

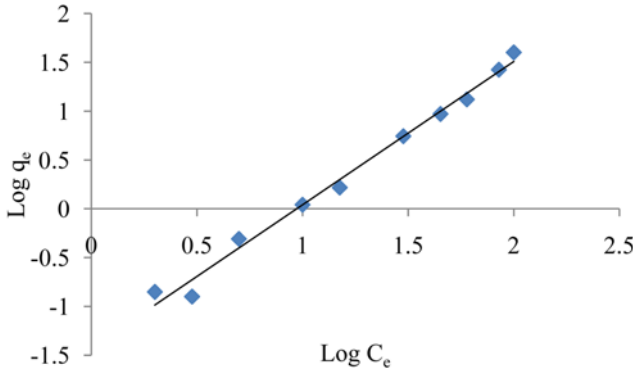

Fig. 10. Freundlich model for biosorption of Cu^{2+} on GPAS.

Table 4. Comparison of Cu(II) adsorption capacities of GPAS with literature

Biosorbent	q_{max} (mg/g)	References
Powdered waste sludge	156.0	[11]
Cladophora Fascicularis	102.24	[14]
Ground Prunus Amygdalus shell (GPAS)	70.16	This study
Marine Macro Algae	62.87	[26]
Waste brewery yeast	48.9	[13]
Tectona grandis leaves powder	15.43	[8]
Myriophyllum spicatum	12.07	[27]
Moss	11.1	[10]
Biomatrix (Rice Husk)	10.92	[17]
Saw dust	4.9	[10]

In Table 4, a comparison of Cu(II) adsorption capacity calculated from Langmuir isotherm on GPAS and other biosorbents is presented. It can be seen that GPAS has good uptake capacity with 70.16 mg/g as compared to other natural biomasses. It indicates that Cu(II) can be easily adsorbed onto GPAS.

4-2. Scatchard Plot

An interpretation about the binding site heterogeneity has been proposed by Dahlquist and Scatchard [28]. According to them the shape of the plot between q_e/C_e versus q_e can be a guide about the nature of the sites. A linear trend indicates the involvement of identical sites; a convex bend shows a single group biding with positive cooperativity while concave curvature presents biding with a negative cooperativity between strong and weak binding groups. In the light of Scatchard and Dahlquist interpretation, the trend of Fig. 11 may be explained as a nonlinear behavior which suggests that biosorption of Cu^{2+} involved non-identical functional groups while concavity of the trend suggests the non-cooperativity of the binding sites [17]. This plot may be taken as a support to the Freundlich isotherm as it also presents the site heterogeneity.

5. Mechanism of Biosorption

To determine the nature of biosorption of Cu(II), i.e., whether it is chemisorption or physisorption, the Dubinin-Radushkevich (D-R) model was studied [3]. This model has following linearized form:

$$\ln q_e = \ln q_{DR} - k_d \varepsilon^2 \quad (10)$$

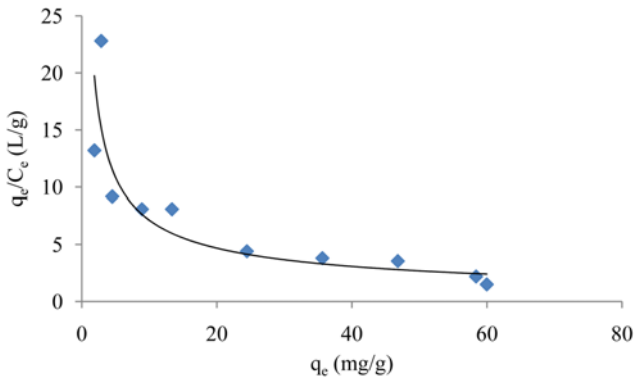

Fig. 11. Scatchard Plot for Cu^{2+} biosorption on GPAS.

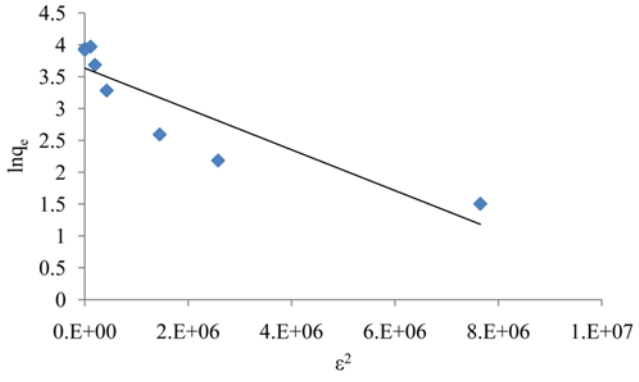

Fig. 12. D-R model for biosorption of Cu(II) onto GPAS.

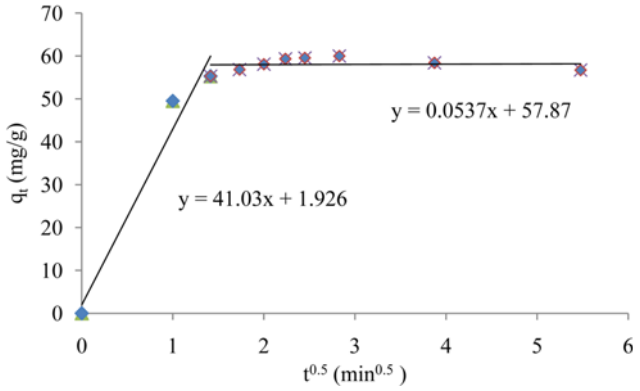

Fig. 13. Pore diffusion model for Cu^{2+} biosorption on GPAS.

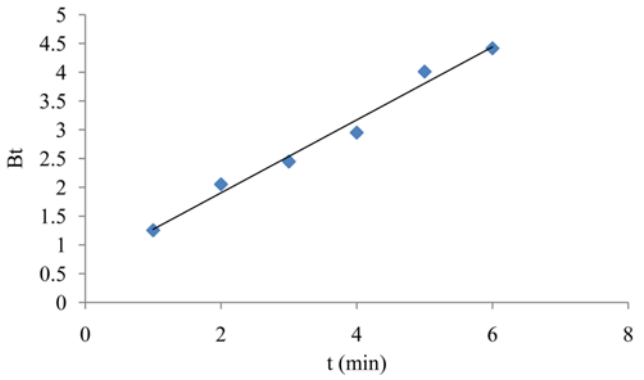

Fig. 14. Boyd plot for Cu^{2+} biosorption onto GPAS.

The parameter k_d, which is obtained from the slope of the graph between $\ln q_e$ and ε^2 as shown in Fig. 12, is used to calculate the energy of adsorption (E). If the value of E is between 1-8 KJ·mol^{-1}, the adsorption will be considered physical, but if it is between 8-16 KJ·mol^{-1}, adsorption will be chemisorption. In the case under consideration value of E is 2.33 KJ·mol^{-1} which means biosorption of Cu(II) onto GPAS is physisorption.

From a mechanistic perspective, in addition to nature of biosorption, i.e., multilayer or monolayer, physical or chemical, it is indispensable to recognize the steps involved during the phenomenon of biosorption. External mass transfer (boundary layer diffusion) followed by intraparticle diffusion are two prominent steps involved in the Biosorption phenomenon. Following equation has been proposed by Weber and Morris for intraparticle diffusion to be the rate controlling step [29]:

$$q_t = k_{id} t^{0.5} + C \quad (11)$$

Where K_{id} (mg·g^{-1}·min$^{-1/2}$) is the intraparticle diffusion constant and C is a constant related to extent of boundary layer thickness. A plot between q_t and $t^{0.5}$ is as shown in Fig. 13.

The trend in Fig. 13 shows multilinearity, which suggests that more than one step is involved in the removal of Cu^{2+} by GPAS. Similar pattern is reported elsewhere [21]. It may be concluded that biosorption of Cu^{2+} on GPAS consists of two steps: sorption on the biosorbent surface followed by the intraparticle diffusion [21]. To determine whether surface biosorption or intraparticle diffusion is the rate controlling step, the model of Boyd plot was studied [18]. According to Boyd model following approximations may be used to determine the rate controlling step.

$$\text{For F values} < 0.85 \quad Bt = 6.28318 - 3.2899F - 6.28318(1 - 1.0470F)^{1/2} \quad (12)$$

$$\text{And for F values} > 0.85 \quad Bt = -0.498 - \ln(1 - F) \quad (13)$$

$$\text{Where } F = \frac{q_t}{q_e} \quad (14)$$

Bt is a function of F which is called fractional attainment of equilibrium at different times, t.

Fig. 14 shows the Boyd plot of Cu(II) biosorption onto GPAS at 30 °C. The rate controlling steps are as shown in Fig. 12.

Boyd model is based on the assumption that pore diffusion is the rate controlling step. As can be seen from Fig. 14, the graph does not pass through the origin, suggesting that instead of pore diffusion, surface diffusion is the rate controlling step. Value of B can be used to calculate effective diffusion coefficient D_i ($cm^2 \cdot s^{-1}$) using following Eq. (14) as below:

$$B = \frac{\pi^2 D_i}{r^2} \quad (15)$$

Where r is the radius of biosorbent particle. The estimated values of diffusion coefficient depending upon different diameters are given in Table 5.

Table 5. Estimation of diffusion coefficient based on various mean diameters

Type diameter	Value of mean diameter (mm)	Diffusion coefficient ($cm^2 \cdot s^{-1}$)
Meadian (From Fig. 1)	0.041	6.36×10^{-7}
Volume mean ($\overline{D}_v$)	0.039	5.76×10^{-7}
Surface volume mean ($\overline{D}_s$)	0.05	9.46×10^{-7}
Mass mean ($\overline{D}_m$)	0.091	0.313×10^{-7}

CONCLUSIONS

GPAS emerged as a potential biosorbent for the removal of Cu(II), as it removed very quickly more than 50% of Cu(II) from synthetic solution. Cu(II) biosorption onto GPAS was found to follow pseudo-second order kinetics. GPAS showed a good tendency to remove Cu(II) at various mass transfer gradients as can be seen from the equilibrium study curve. Fitting of equilibrium models and Scatchard plot revealed the possibility of heterogeneity of the binding sites. Carboxylic and alcoholic groups were indicated by the FT-IR as the main functional groups which may play a role to remove Cu(II) from synthetic solution. XRD showed the vagueness of the biosorbent. Size analysis revealed that volume mean diameter described best the average size of GPAS, which was in conformation to the SEM image. Surface diffusion was found to be the rate controlling step and diffusion coefficient was estimated based on different diameters calculated.

ACKNOWLEDGEMENT

The support of the Department of Chemical Engineering, University of Engineering & Technology Lahore is highly acknowledged.

REFERENCES

1. B. Volesky and Z. R. Holan, *Biotechnol. Prog*., **11**, 235 (1995).
2. K. S. Rao, S. Anand and P. Venkateswarlu, *Korean J. Chem. Eng*., **27**(5), 1547 (2010).
3. C. S. Zhu, L. P. Wang and W. J. Chen, *J. Hazard. Mater*., **168**, 739 (2009).
4. B. Volesky, *Hydron*., **59**, 203 (2001).
5. C. Jeon, J. Y. Park and Y. J. Yoo, *Korean J. Chem. Eng*., **18**(6), 955 (2001).
6. R. Han, L. Zhang, C. Song, M. Zhang, H. Zhu and L. Zhang, *Carbohyd. Polym*., **79**, 1140 (2010).
7. E. Pehlivan, T. Altun, S. Cetin and M. I. Bhanger, *J. Hazard. Mater*., **167**(1-3), 1203 (2009).
8. Y. P. Kumar, P. King and V. S. R. K. Prasad, *J. Hazard. Mater*., *B*, **137**, 1211 (2006).
9. B. Volesky, Bv sorbex Inc., Montreal, 35 (2003).
10. A. Grimm, R. Zanzi, E. Bjornbom and A. L. Cukierman, *Bioresour. Technol*., **99**, 2559 (2008).
11. M. Y. Pamukoglu and F. Kargi, *Process Biochem*., **41**, 1047 (2006).
12. E. Pehlivan and T. Altun, *J. Hazard. Mater*., **155**, 378 (2008).
13. T. Y. Kim, S. K. Park, S. Y. Cho, H. B. Kim, Y. Kang, S. D. Kim and S. J. Kim, *Korean J. Chem. Eng*., **22**(1), 91 (2005).
14. L. Deng, Y. Su, H. Su, X. Wang and X. Zhu, *Adsorption*, **12**, 267 (2006).
15. Y. N. Mata, M. L. Blazquez, A. Ballester, F. Gonzalez and J. A. Munoz, *J. Hazard. Mater*., **158**, 316 (2008).
16. S. Gupta and B. V. Babu, *Chem. Eng. J*., **150**, 352 (2009).
17. K. K. Krishnani, X. Meng, C. Christodoulatos and V. M. Boddu, *J. Hazard. Mater*., **153**, 1222 (2008).
18. K. Li and X. Wang, *Bioresour. Technol*., **100**, 2810 (2009).
19. B. N. Estevinho, N. Ratola, A. Alves and L. Santos, *J. Hazard. Mater.*, *B*, **137**, 1175 (2006).
20. H. H. Acma and S. Yaman, *Fuel*, **86**, 373 (2007).
21. K. V. Kumar and K. Porkodi, *J. Hazard. Mater*., **146**, 214 (2007).
22. W. L. Mcabe, J. C. Smith and P. Harriot, *Unit operations of chemical engineering*, 7th Ed., McGraw Hill Inc. (2005).
23. N. P. Dalmini, B. B. Mamba and A. F. M. Bafubiandi, *Water S.A*., **36(**4), 445 (2010).
24. K. Y. Foo and B. H. Hameed, *Chem. Eng. J*., **156**, 2 (2010).
25. J. Febrianto, A. N. Kosasih, J. Sunarso, Y. H. Ju, N. Indraswati and S. Ismadji, *J. Hazard. Mater*., **162**, 616 (2009).
26. Q. Yu and P. Kaewsarn, *Korean J. Chem. Eng.*, **16**(6), 753 (1999).
27. G. Li, P. Xue, C. Yan and Q. Li, *Korean J. Chem. Eng*., **27**(4), 1239 (2010).
28. F. W. Dahlquist, *Methods of Enzymology*, Academic Press, New York, 270 (1978).
29. W. J. Weber and J. C. Morris, *J. Sanit. Eng. Div. A.S.C.E*., **89**, 31 (1963).